ornl

ORNL/TM-8254

OAK
RIDGE
NATIONAL
LABORATORY

UNION
CARBIDE

Elevated-Temperature Deflection-Controlled Test of Modified 9 Cr–1 Mo Steel Beam

R. C. Gwaltney
R. L. Battiste
G. T. Yahr
M. L. Peters

Full release per David Hamrin 7/17/13

[redacted]

OPERATED BY
UNION CARBIDE CORPORATION
FOR THE UNITED STATES
DEPARTMENT OF ENERGY

Printed in the United States of America. Available from
the U.S. Department of Energy
Technical Information Center
P.O. Box 62, Oak Ridge, Tennessee 37830

ORNL/TM-8254
Dist. Category UC-79T,
-79Th, -79Tk
OR-1.7.3 Advanced Alloy
Technology: Design
Methods

Contract No. W-7405-eng-26

Engineering Technology Division

ELEVATED-TEMPERATURE DEFLECTION-CONTROLLED TEST OF MODIFIED 9 Cr-1 Mo STEEL BEAM

R. C. Gwaltney G. T. Yahr
R. L. Battiste M. L. Peters

Date Published — May 1983

NOTICE This document contains information of a preliminary nature. It is subject to revision or correction and therefore does not represent a final report.

Prepared by the
OAK RIDGE NATIONAL LABORATORY
Oak Ridge, Tennessee 37830
operated by
UNION CARBIDE CORPORATION
for the
U.S. DEPARTMENT OF ENERGY

CONTENTS

ELEVATED-TEMPERATURE DEFLECTION-CONTROLLED TEST* OF MODIFIED 9 Cr-1 Mo STEEL BEAM

R. C. Gwaltney G. T. Yahr
R. L. Battiste M. L. Peters†

ABSTRACT

This report presents elevated-temperature test results and comparisons with analytic predictions for a simply supported modified 9 Cr-1 Mo steel beam subjected to a controlled center deflection history. The test was performed to provide an assessment of structural analysis methods and material relations for modified 9 Cr-1 Mo steel. The inelastic analysis predictions were obtained using the finite-element code ADINA. The analysis was done using a nonlinear, time-independent plasticity model and a creep strain-hardening model for the constitutive equations. The test contained three constant-deflection hold periods for a total of 504 h at a temperature of 573°C (1100°F).

The beam specimen was fabricated using plate stock of the modified 9 Cr-1 Mo steel at heat 30383. The structural deformation responses in terms of load and strain were measured during the test; results are provided in graphical form. The analytical and experimental results are in reasonably good agreement, but further development of the constitutive relations and/or analytical methods is indicated.

Keywords: beam, 9 Cr-1 Mo steel, structural test, high-temperature structural design, LMFBR, inelastic analysis, finite element, plasticity, creep.

---

1. INTRODUCTION

Only through comparisons with data from structural tests can constitutive equations and analytical methods be assessed in terms of validity and accuracy. The Department of Energy (DOE) and its predecessors have been very active since 1969 in providing experimental test data and assessing the validity and accuracy of the analytical methods required for high-temperature structural design of liquid-metal fast breeder reactor (LMFBR) system components.

---

*Work performed under DOE/OBTP AF 15 40 10 3, Task No. OR-1.7.3 Advanced Alloy Technology: Design Methods.

†Student at University of Minnesota at River Falls.

A simply supported beam loaded at the center is one of the simplest possible types of structural tests for investigating inelastic structural behavior. This simple structural test involves nonhomogeneous and statically indeterminant stress fields such that nontrivial inelastic analysis (typically accomplished by using finite-element computer programs) is needed to predict behavior based on uniaxial materials data. Yet, the model is two-dimensional (plane) and thus relatively inexpensive to analyze. This simple structural test exhibits many of the essential features of high-temperature structural behavior: time-varying inelastic strain concentrations, elastic follow-up, and accumulated inelastic strain. Because of simplicity, this test is potentially more accurately controlled and monitored, it is less expensive to conduct, and the collection and interpretation of the test data are more easily managed.

The beam test may be thought of as a first step beyond the usual material test in which stresses are statically determinant from the applied loads. The beam has essentially a uniaxial stress field, but the field is nonhomogeneous. Furthermore, both the stress and strain distributions change with inelastic deformation and time and can only be determined by analysis.

The test covered in this report is of a simply supported modified 9 Cr—1 Mo steel beam subjected to a controlled center deflection at an elevated temperature. Complete test results are presented in graphical form and discussed. Comparisons with detailed elastic—plastic creep analyses are presented and discussed. The detailed analysis was performed with the computer program ADINA (Ref. 1), although a second confirmatory analysis using CREEP—PLAST II is presented in an appendix.

The remainder of this report is arranged in seven sections. Section 2 describes the test specimen in terms of dimensions, material, and fabrication. The experimental facility is discussed in Sect. 3, while Sect. 4 discusses the specimen instrumentation. Section 5 discusses the test histogram and procedures, and Sect. 6 details the analysis methods and procedures employed in the study. Section 7 compares the experimental and analytical results. Finally, Sect. 8 provides a summary.

2. BEAM DESCRIPTION

The beam specimen was a simply supported, centrally deformed beam (displacement control) of uniform rectangular cross section as shown in Fig. 1. The specimen was 51.39 mm (2.035 in.) high, 26.24 mm (1.033 in.) wide, 0.66 m long (nominally 1 x 2 x 26 in.), and simply supported so that the effective length was 0.61 m (24. in.). The center deflection was applied through a 19-mm-diam (0.75-in.) roller downward (+P) on the top surface or upward (-P) on the bottom as shown. The simple end supports were through 19-mm-diam (0.75-in.) rollers that passed through the beam on its center line.

A schematic indicating the instrumentation used for measuring deflection, strain, and temperature is shown in Fig. 2. Details of the instrumentation are discussed in a later section. The material for the beam specimen was 25-mm (1-in.) plate stock of modified 9 Cr—1 Mo steel (heat 30383). The heat treatment of the beam involved normalizing at 1038°C (1900°F) for 1 h, followed by air cooling. It was tempered at 760°C (1400°F) for 1 h, followed by air cooling to room temperature.

ORNL-DWG 74-13291

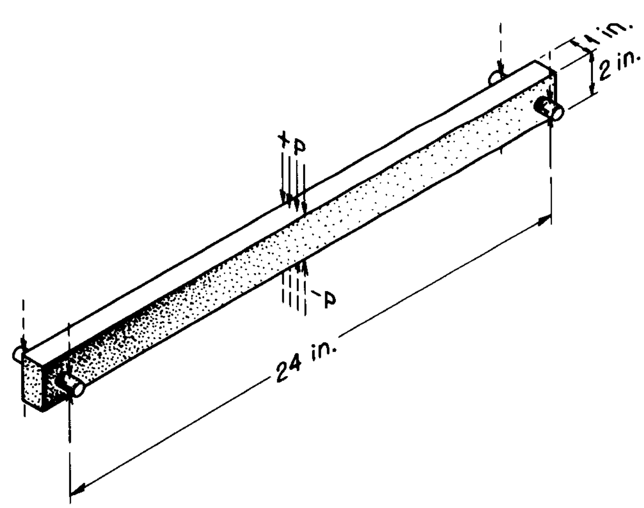

Fig. 1. Simply supported beam specimen [dimensions shown are nominal (1 in. = 25.4 mm)].

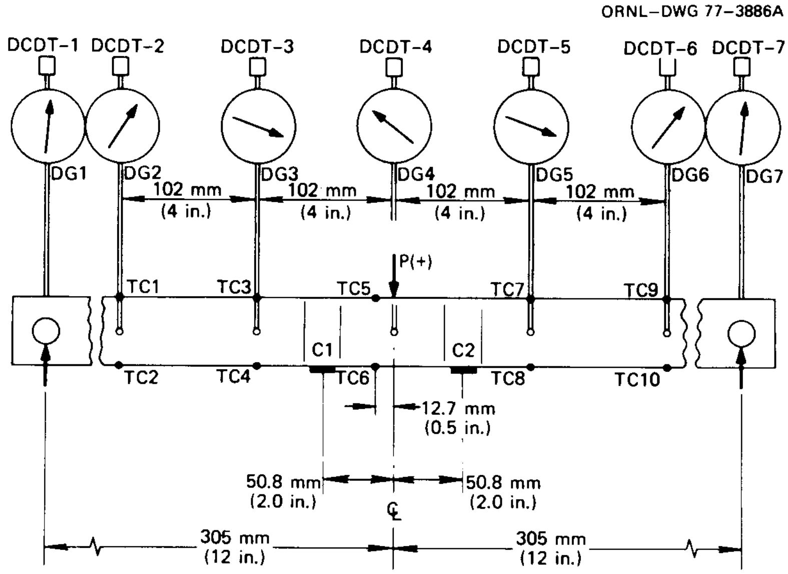

DCDT: DISPLACEMENT TRANSDUCER
DG: DIAL GAGE
TC: THERMOCOUPLE
C: BOEING/HITEC CAPACITIVE STRAIN GAGE

Fig. 2. Schematic of instrumentation.

3. EXPERIMENTAL FACILITY

3.1 Beam Test Facility

A special elevated-temperature test facility was designed and built specifically for testing beams. The beam loading system can be divided into three major subsystems: the load frame, the hydraulic power supply, and the control system. The load frame is shown schematically in Fig. 3 with a three-point loaded beam specimen installed. For long-term constant-load creep periods, a system of dead weights acting through cables, pulleys, and a bell crank arrangement was used to apply a vertical load up or down through the creep loading arms shown on each side of the loading

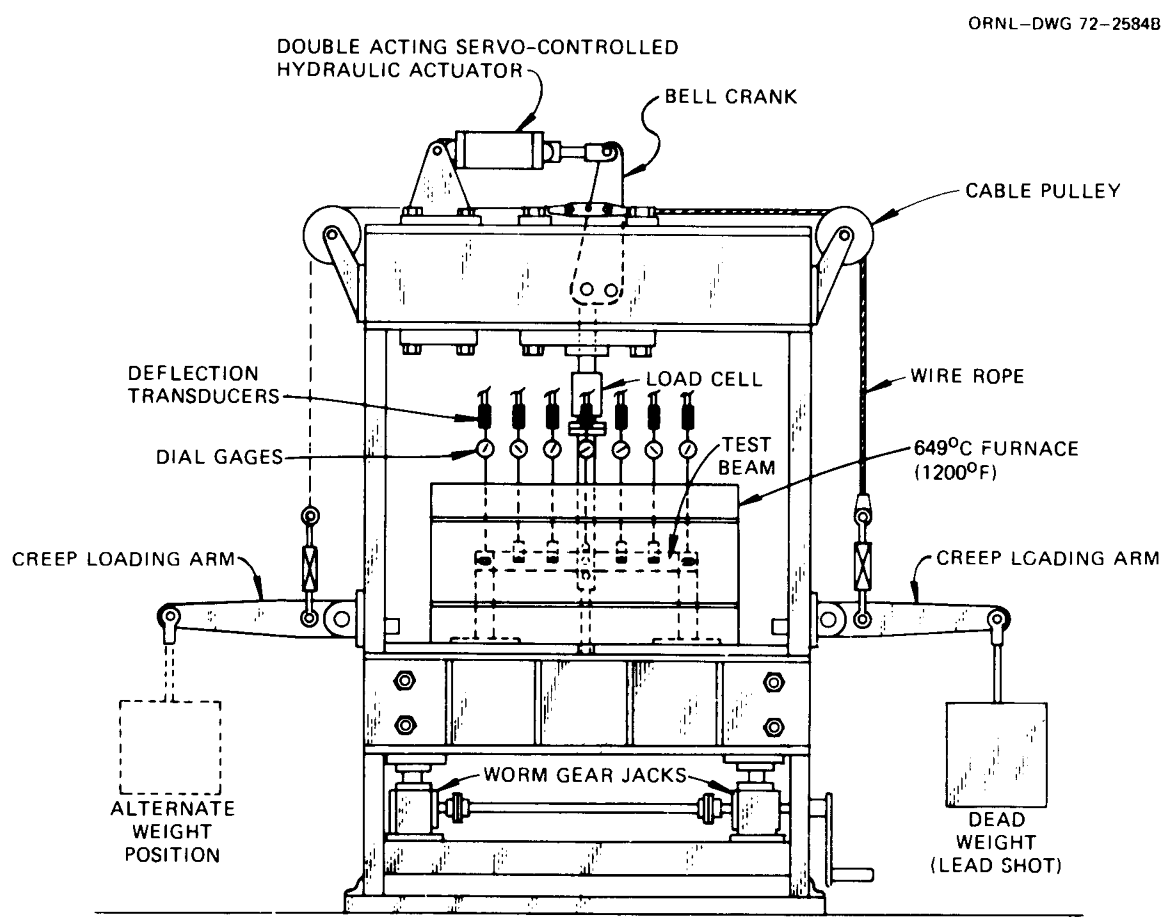

Fig. 3. Schematic drawing of elevated-temperature beam test facility.

frame. This dead weight system provided a mechanical advantage of 14 to 1. The double-acting hydraulic actuator was operated as a trimmer system at reduced pressure during the creep periods to overcome the relatively small effects of friction in the dead weight system. For short-time cycling and load changes and for all deflection-controlled testing, the creep loading arms were disconnected, and the hydraulic actuator was utilized. The hydraulic actuator-bell crank arrangement provided a 4-to-1 mechanical advantage. The load was transmitted through the beam support system (see Fig. 4) to the specimen.

ORNL-DWG 79-16763R ETD

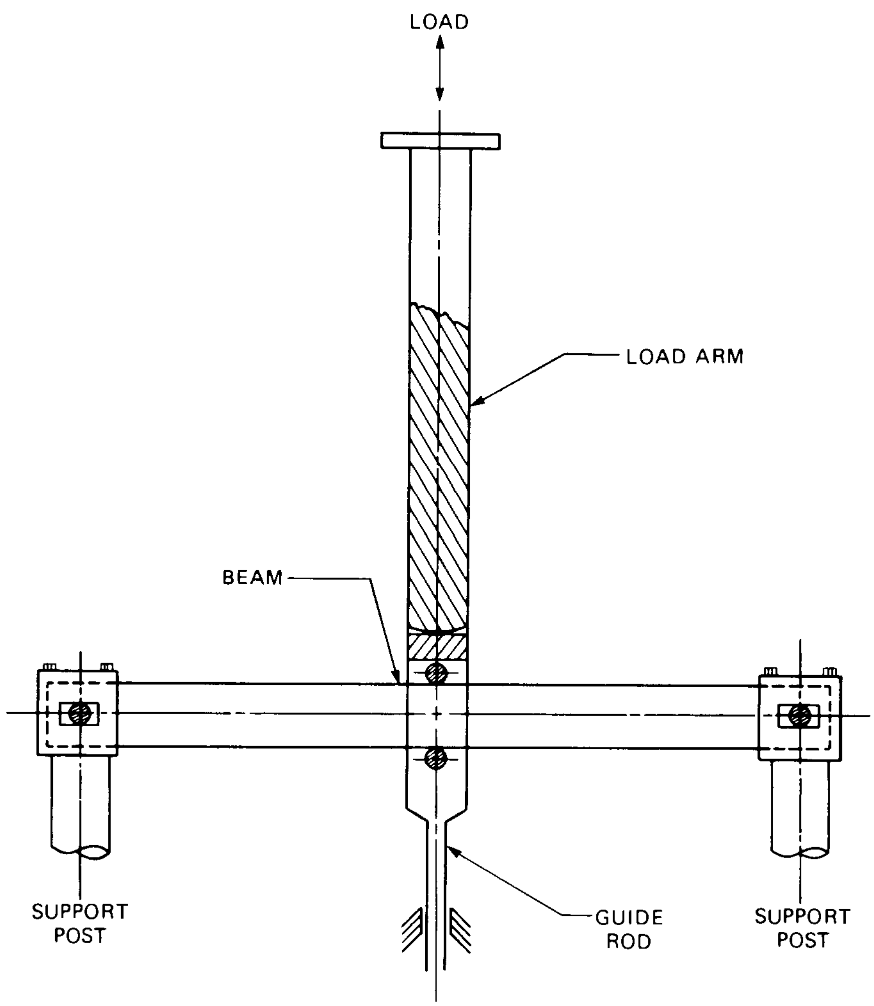

Fig. 4. Schematic of beam support system.

The support system consisted of a load arm and two end support posts. The material for these three parts was 304 stainless steel. The dowel pins through each end of the beam specimen and the two dowel pins in the load arm were Inconel Alloy X-750. The end post dowel pins were 50.8 mm (2 in.) long and 19 mm (0.75 in.) in diameter, while the loading fixture pins were 28.6 mm (1.125 in.) long and 19 mm (0.75 in.) in diameter. The pins were solution annealed prior to the test by heating to 982°C (1800°F) and holding for 1 h, air cooling to 732°C (1350°F) and holding for 8 h, furnace cooling to 621°C (1150°F) and holding for 18 h, and furnace cooling to room temperature. The end post slots were faced with thin 3.2-mm (0.125-in.) Stellite inserts, top and bottom, which contacted the beam support dowels. The slots helped to prevent extraneous loading of the beam during heatups and cooldowns. Also, the inserts and the increased yield strength, resistance to creep, and hardness of the dowel pins due to their heat treatment helped ensure proper application of the loads (correct boundary conditions) and prevented problems of self welding during long-term high-temperature tests. An extension guide rod mechanism, which attached to the loading fixture and passed through a cylindrical bushing on the reaction surface of the loading frame below the beam, was used to maintain alignment of the center loading fixture.

The hydraulic power supply was a 600-series Denison hydraulic pump with a variable-volume cylinder control. A Denison pressure relief valve, which was an integral part of the pump, was adjusted until a constant output of pressure of 6.895 MPa (1000 psig) was achieved, and the variable-volume control was set to one-fourth volume flow, 10.2 L/min (2.76 gpm) at 6.895 MPa (1000 psig). An 11.4-L (3-gal) Greer accumulator with a precharge of 2 MPa (300 psig) was installed to dampen pressure fluctuations. The pump was protected by low-level and high-temperature alarms and interlocks. A check valve and a 0.95-L (1-qt) Greer accumulator were mounted at the facility to provide hydraulic insulation from other facilities serviced by this hydraulic power supply and to provide pressure for an orderly shutdown in emergency situations.

A closed-loop servocontrol system was used that consisted of an MTS model 442 servocontroller, an R.I. model FGE 5110 Data-Trak programmer, a master control panel, a Moog model 73-100 servovalve, two high-pressure solenoid valves, a hydraulic actuator, and a strip chart recorder. The MTS controller used two signals – command and feedback – to develop a control signal that operated the servovalve. The command signal was a composite of a static level, a set point potentiometer provided by the controller, and a programmable signal generated externally by the Data-Trak. The command signal represented the desired or programmed condition of the controlled variable. The feedback signal represented the actual condition of the controlled variable. If command and feedback were not equal, an error signal was developed, amplified, and applied to the servovalve as a control signal. The servovalve opened, allowing high-pressure oil to flow into the hydraulic actuator in a direction required to bring the mechanical input to the feedback transducer back to the command level. One of three independent feedback transducers – a load cell, a displacement transducer, and a strain gage – could manually be selected through the MTS controller. Also, the outputs of two of the three transducers were selectable as inputs to the Hewlett-Packard Model 7100B strip chart recorder, and one output could be selectively monitored on a panel-mounted digital voltmeter.

During the test, which was deflection-controlled, the output of a direct-current differential transformer (DCDT) displacement transducer was used as the feedback transducer. An Oak Ridge National Laboratory (ORNL) module that was compatible with the MTS controller provided a small zero adjustment and four selectable ranges of gains of 1, 2, 5, and 10. A gain of 2 was selected for use with the DCDT displacement transducer system.

The Data-Trak programmer was an electromechanical instrument designed to position the shaft of a precision potentiometer in accordance with variations in a preplotted program attached to a rotating drum. The desired program curve was inscribed in the metallized surface of a special program chart with a stylus that divided the chart into two electrically isolated conductive plates. A servodriven probe would follow the curve by seeking the zero potential existing at the center of the program curve. The shaft of the output potentiometer was mechanically coupled to the probe through a system of pulleys. The potentiometer was excited by a $\pm$10-V reference voltage supplied by the MTS controller. Therefore, as the probe was driven to follow the program curve on the rotating drum, the position of the potentiometer wiper varied accordingly, producing an electrical signal that was the mirror image of the program curve.

The master control panel was a switching center that coupled the hydraulic power supply, the control system, and the two solenoid valves. The hydraulic power supply could be started and stopped from the panel. The master panel had fail-safe interlocking circuits that opened when an abnormal condition existed. When the interlock opened, the hydraulic power supply was automatically shut down and the solenoid valves were closed. These solenoid valves were located at each end of the hydraulic actuator, thus producing an instantaneous stop-action situation for the actuator. Some of the abnormal conditions were low fluid level and an over-temperature in the hydraulic power supply, depression of the emergency stop switch, and a deviation alarm. The deviation alarm was generated by the MTS controller when the feedback signal differed from the command signal by a preset amount, ~5% for this controller.

3.2 Temperature System Control

The furnace structure consisted of light stainless steel frame sections filled with 127 mm (5 in.) of high-temperature insulation and lined on the inside with perforated stainless steel sheet metal. Flat serpentine resistance rod heaters (230-V Calrods) attached to the four inside wall sections provided up to 6 kW of heat. Temperature control was provided by an ORNL-designed three-zone control system that utilized three Leeds and Northrup Electromax III temperature controllers. The feedback signals were provided by Chromel-Alumel thermocouples mounted on both end posts and on the beam 305 mm (12 in.) from one end. The current output of the controllers drove zero-voltage power supplies (L&N model 11906-233 Power Packages). The outputs of the power supplies were passed through variable auto transformers (Superior Electric Powerstats) before going to the heater elements. Each zone was limited to a maximum output of ~2 kVA by the 9-A transformers, but these transformers provided the versatility required to balance the heat load and obtain a uniform temperature distribution. Also, 6 kVA was more than enough power for the beam specimen. Over-temperature protection for each zone was provided by Con Ohmic alarm modules and transmitter-amplifier modules that used a second Chromel-Alumel thermocouple for each zone. The furnace and control systems were capable of controlling temperatures within ±2.8°C (±5°F) over a temperature range of 425 to 625°C (800 to 1250°F) under almost any condition.

3.3 Data Acquisition System

The high-temperature structural test data acquisition system (DAS) was a Hewlett-Packard model 9603 A measurement and control system, and its components are listed in Table 1. The system was based on a Hewlett-Packard 1000 Series computer with 256 kilobytes of memory. The nucleus of the software system was Hewlett-Packard's memory-based real-time executive system, RTE-IVB, which operates in the Fortran language. The operating program was written by High-Temperature Structural Design (HTSD) Technology Program personnel, which facilitated onsite program modification and data reduction. Raw voltage data were recorded in real time on industry-compatible magnetic tape, which facilitated detailed analysis on the IBM 3330 computer in the ORNL Computing Center. Preliminary data analysis could be performed locally and displayed on site via system console.

Table 1. Components of the HTSD DAS

Item	Quantity	Description
1	1	HP 1000 Series model 2117F computer with 256 kilobytes of memory
2		7925 Disc with 120 megabytes of memory
3	1	Time base generator HP part No. 12539C
4	2	Magnetic tape unit, HP part No. 7970B
5	1	2648 Graphic System console
6	1	Punch tape reader, HP part No. 2748B
7	1	Paper tape punch, HP part No. 2895B
8	1	Analogue signal input system, HP part No. 02313B

This DAS was capable of scanning, digitizing, and recording dc voltage signals for 144 separate sensor signals in the range of ±10 mV dc to ±10 V dc. The multiplex rate for the ±10-V range was 45,000 channels per second, and for all other ranges it was 8000 channels per second. The overall system accuracy for all possible ranges is listed in Table 2. The system's maximum scanning rate was 50 scans (samples) per second, although the system was used at an actual maximum scan rate of ~1 scan per second.

Table 2. HTSD DAS accuracy and temperature coefficient by input ranges

Input ranges (mV)	Overall accuracy[a] (% full scale ±1/2 least significant bit) for sample rates to		Temperature coefficient (% full scale/°C)
	20 Hz	50 Hz	
±10	±0.33	±0.38	±0.0054
±20	±0.28	±0.31	±0.0054
±40	±0.23	±0.26	+0.0054
±80	±0.19	±0.21	±0.0054
±100	±0.17	±0.19	±0.0064
±200	±0.15	±0.16	±0.0064
±400	±0.14	±0.16	±0.0064
±800	±0.14	±0.15	±0.0064
±10	±0.09	±0.09	±0.0026

[a]Factors included: three-sigma noise; linearity; offsets; 8-h stability; gain, calibration transfer, and dynamic response errors; and effects of ±10% line voltage variation and ±5°C variation from calibration temperature.

One of the three scan modes (high-speed, averaging, and single) was automatically chosen and executed by the data acquisition operating program when a scan sequence was requested. The high-speed scan mode was executed when a periodicity of <1 min was specified, and the averaging mode was executed for periodicities of ≥1 min. The averaging and single scan modes improved the system accuracy by averaging ten scans and recording the results on magnetic tape. The ten scans were taken and stored in memory in <10 s.

4. SPECIMEN INSTRUMENTATION

The instrumentation used for measuring deflection, strain, and temperature in this test was shown in Fig. 2. The specimen had seven displacement-measuring devices and two Boeing-HITEC capacitive strain gage systems. Also, ten thermocouples were located on the top and bottom surfaces. Readings from the load cell (Fig. 3), displacement devices, strain gages, and thermocouples were recorded on the DAS.

A single-bridge 44-kN (10,000-lb), U-1 Model SR-4 load cell was used in the beam test. The single bridge required dedication to the DAS. The load cell was calibrated at a standards laboratory before the test and rechecked prior to the test using a BLH model 625 precision calibrator. The bridge sending signals to the DAS was excited by an Endevco model 4470 signal conditioner module.

The displacement measurement was done with a Hewlett-Packard model 24 DCDT displacement transducer. The maximum nonlinearity was $\pm 0.5\%$ of full scale, and the sensitivity was ± 5 V dc for full-scale strokes for all DCDT transducers. Excitation was provided by a single Hewlett-Packard model 6205B power supply.

These displacement transducers are linear-variable differential transformers with built-in dc-excited carrier oscillator and phase-sensitive demodulator systems. A DCDT transducer consists of a coil assembly and a core that, when displaced linearly along the axis and within the bore of the coil assembly, produces a voltage change in the output proportional to the displacement.

A DCDT coil assembly consists of a differential transformer coil, a dc-excited solid-state oscillator, and a phase-sensitive demodulator all in one package. The oscillator converts the dc input power to ac, which is used to excite the primary winding. The axial core position determines the amount of voltage induced in the secondary windings. Each of the two secondary circuits contains a secondary winding, a full-wave bridge, and an RC filter. These secondary circuits are connected in series opposition so that the resultant output is a dc voltage proportional to the core displacement from electrical center. The polarity of the voltage is a function of the location of the core with respect to electrical center. Input and output circuits are electrically isolated, but not totally isolated, from each other and the coil assembly case. This insufficient isolation causes noise problems when several transducers are excited by a common power supply and when ground paths between the transducers exist, which is the exact application used in these tests. It was necessary to physically isolate each transducer coil assembly and core so no common ground path existed and to filter the output with a 1-kHz filter developed by ORNL Instrumentation and Controls Division personnel. Tests were performed to ensure that the frequency response of the transducer systems, with this external filtering, was adequate to track the structural behavior expected in these tests and to produce undistorted displacement measurements.

Dial gages were used in series with the DCDT transducers as backup (see Fig. 2). The DCDT transducer cores, the dial gage operator shafts, and the quartz rods (which extended to the specimen inside the test furnace) were coupled using special adapters (see Fig. 5). The quartz rods and dial gages were spring loaded to ensure continuous contact with the specimen. For positions 2, 3, 5, and 6, the quartz rods were seated in saddles (Fig. 5) that were attached to the midsurface of the beam, while the rods for positions 1 and 7 bore directly on the top surface. The center rod (position 4) was attached to the beam on only one side at the midsurface (Fig. 5).

The dial gage and DCDT displacement transducer assemblies were calibrated using a Boekeller micrometer. The micrometer was calibrated at a standards laboratory using remote interfermetry, specifically with a Go-Devil linearity checker. The absolute accuracy of the assemblies was not exactly quantifiable but better than ±0.125 mm (±0.005 in.), which included temperature effects and rigid body movements. The resolution was 0.0125 mm (±0.0005 in.) including the DAS, and the indicated accuracy was better than ±0.055 mm (±0.002 in.).

The strain transducers were Boeing-HITEC differential capacitive strain-gage systems. Basically, the system consists of surface and signal-conditioning modules that generate ac excitation for the gage and demodulate the gage output, producing an electrical analogue of specimen mechanical strain (see Fig. 6).

ORNL–PHOTO 4032–74

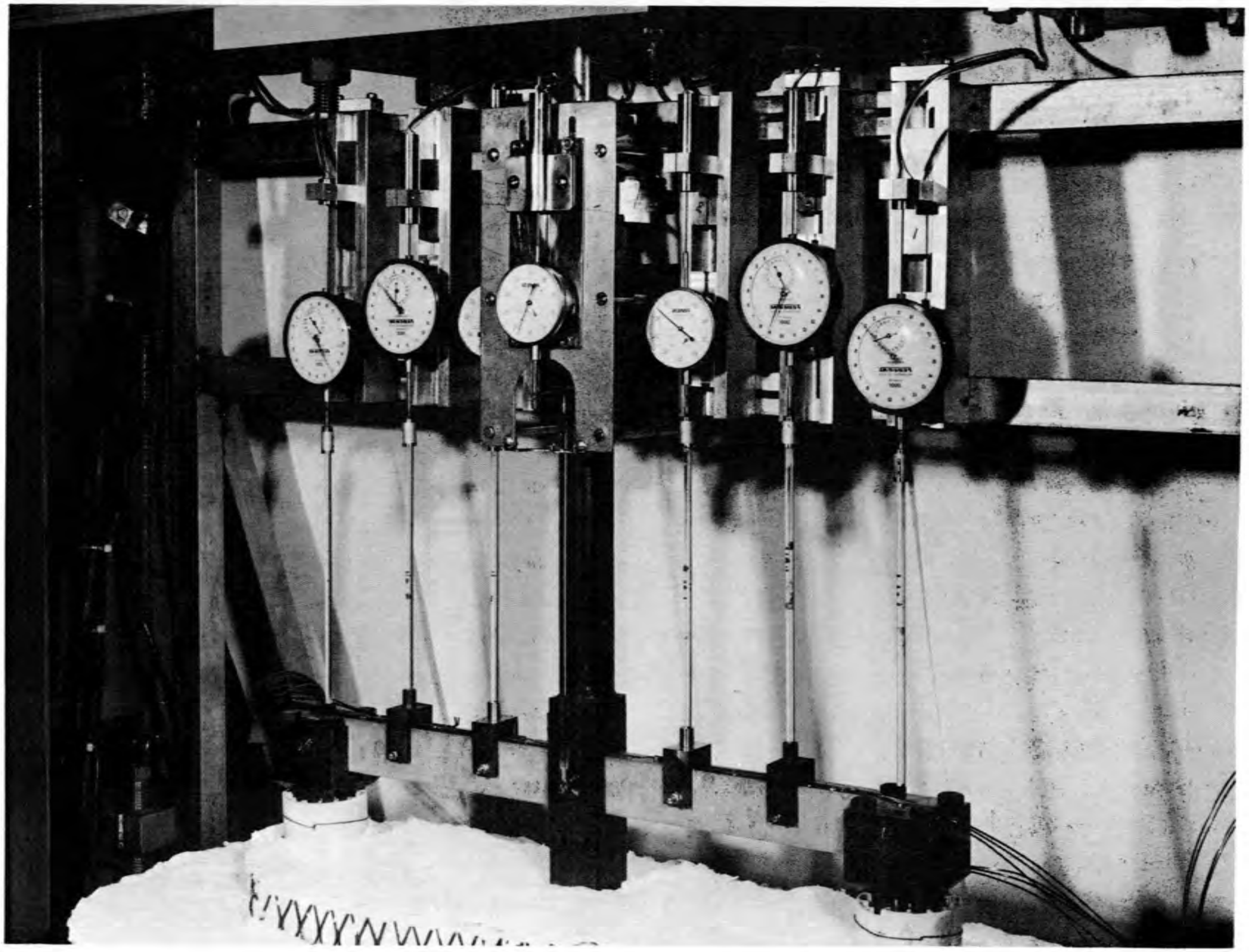

Fig. 5. Instrumented beam mounted in test facility.

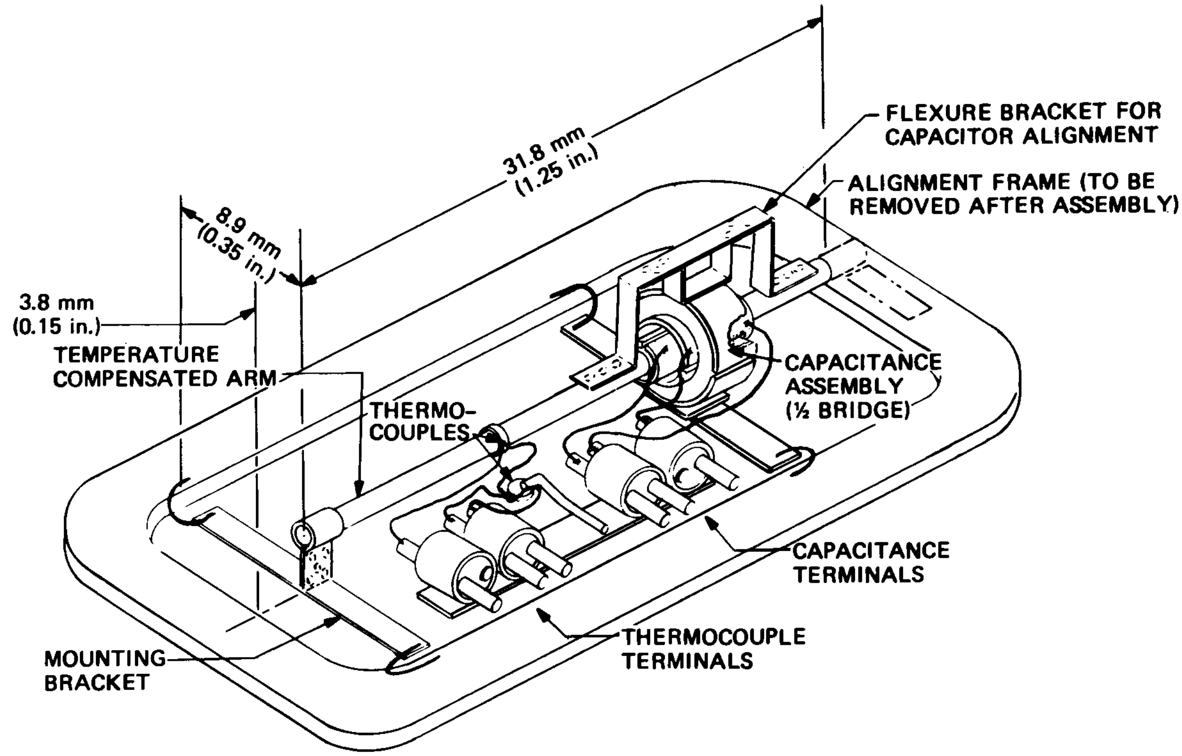

Fig. 6. Schematic drawing of Boeing capacitive strain gage.

The capacitive strain gage consisted electrically of two variable capacitors connected as a half bridge. The capacitor plates were concentric cylinders, and the dielectric was air. The outer cylinder of the gage was capacitively coupled through the air dielectric to each of the two inner cylinders. As the specimen dimensions changed because of strain, the outer cylinder moved axially with respect to the two inner cylinders, changing the capacitance between them differentially.

The cylindrical plates of the capacitors were attached to the specimen by high-temperature alloy ribbon flexures through spot welding. The flexures permitted the gage to retain concentricity and alignment of its capacitor plates regardless of specimen warpage or bending. The capacitor plates were restrained in only one plane, that is, the plane necessary for concentricity. In the direction of strain measurement, which was axial to the capacitor plates, they were free to move throughout the nominal range of the strain gage.

Temperature compensation was achieved by fabricating the rod, which establishes the length dimension of the gage [nominally 2.54 cm (1 in.)], from material with a thermal expansion characteristic identical to that of the material of the specimen. Both the strain gage and the specimen were instrumented with thermocouples to provide data for computing corrections required by any temperature difference between the strain-gage rod and the specimen surface and by any mismatch of gage rod and specimen properties.

The heart of the signal-conditioning system was the mode card, which was designed to work in an Endevco model 4470 module in place of an Endevco mode card. The signal-conditioning mode card received dc power from the Endevco model 4470 module power supply. The mode card in turn applied ac excitation voltage to the capacitive strain gage. To accommodate long cable lengths, the mode card input stage was a charge amplifier, with added filtering designed to suppress power line noise. Demodulation was performed on the mode card, using a multiplier principle. The mode card output was filtered to eliminate excitation-related frequency components.

The gages used in this test had a nominal 2.54-cm (1-in.) gage length and Rene 41 gage rods. Flat shims were attached to the specimen using a single spot weld on each shim, thereby establishing point-to-point strain measurements. The gages were then attached to the shims. HITEC model 4479.6 signal-conditioning mode cards were employed.

The locations of the ten premium-grade type K (Chromel-Alumel) thermocouples (TC-1 through -10) used to obtain experimental data were shown in Fig. 2. The thermocouples were grounded type 310 stainless steel sheathed with MgO insulation, 1.59 mm (0.0625 in.) in diameter x 91.44 cm (36 in.) long, and made to ORNL Instrumentation and Controls Division specification IS-121. They were joined to twisted-pair, double-shielded, equal-resistance extension wires with thermocouple-grade connectors. The signals were referenced to a Research, Inc., 40-point, 65.6°C (150°F) reference junction box that had a specified accuracy of ±0.14°C (0.25°F). With DAS considerations, an indicated error of ±2°C (3.6°F) was obtained in the range of interest, excluding long-term drift. Long-term drift in type K thermocouples cannot be quantified because metallurgical changes in the wire (an ordering effect) prevent correlation of pretest and posttest calibrations.

5. TEST DESCRIPTION AND PROCEDURE

The histogram for the modified 9 Cr–1 Mo test is shown in Fig. 7 and is labeled or numbered for reference and presentation of the results. The test temperature was isothermal [593°C (1100°F)], and the test was center deflection controlled. All short-term load changes were conducted at a rate of 0.13 mm/s (0.005 in./s). The test was composed of three 1-week hold periods (168 h) with two cyclic deflection reversals between hold periods. One hold period deflection was opposite in sign to the other two. The hold periods were controlled at ±2.54-mm (0.1-in.) deflection at the center. The first cyclic loading was at ±2.54 mm (0.1 in.) except for the last tension deflection, which was 5.08 mm (0.2 in.). The second cyclic deflection was at ±5.08 mm (0.2 in.).

A shakedown test on the loading system was performed using a dummy specimen to ensure that the loading was functioning properly and to check the system calibration. Room temperature elastic tests were performed using the actual specimen to ensure proper operation of all instrumentation before heatup. The initial part of the high-temperature test was devoted to verification and stabilization of system parameters. When the

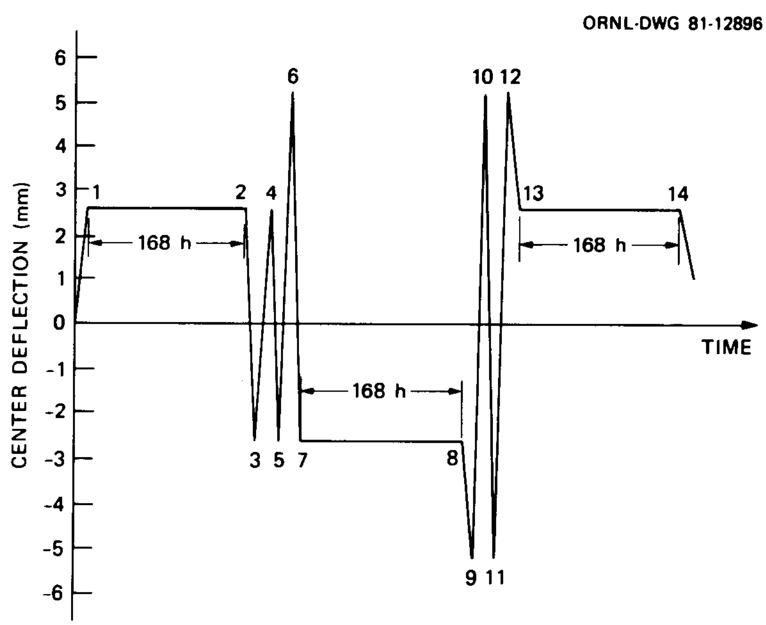

Fig. 7. Deflection histograms for center deflection of beam.

specimen reached the nominal test temperature, the temperature control system was adjusted to establish a uniform temperature distribution. Once a uniform temperature distribution was stabilized, the displacement devices and the strain transducers were adjusted to their respective null positions, and their engineering-units conversion factors were verified. After a 24- to 48-h period to verify that all systems were working properly, the test was initiated.

The DAS was the primary collection point of the experimental data. Scan sequences with a periodicity of 1/s were done during all transients of the control deflection. Backup data were collected on X-Y recorders during the transients to graphically record how the strain and deflection varied with load. Data were collected at necessary intervals to define the specimen behavior during hold periods. Backup data were recorded manually on a daily basis for the hold periods.

The test operated adequately except for an operator error that caused an unrecorded premature deflection of the beam. The DAS was not recording at the time. The unknown loading was removed, but it had created a permanent deflection of 1.054 mm (0.045 in.). The instrumentation on the test performed adequately. The only exception was that the temperature controller had a malfunction, causing a drift in temperature. All of the thermocouple pairs above and below the beam had the same symmetrical drift, except for TC-5 and TC-6. TC-6 was consistently 5°C (41°F) cooler than the operating temperature.

6. ANALYTICAL METHODS AND PROCEDURES

A nonlinear, time-independent plasticity model[2] was used for the plastic inelastic analysis, which incorporates some aspects of both isotropic and kinematic hardening. The model characterizes a material with limited memory, that is, in the sense that part of the deformation history as recorded in the internal dislocation structure is erased at stress reversals. This feature ensures that the predicted response eventually reaches a limit cycle under cycling stressing even in the presence of creep and relaxation.

The nonlinear plasticity model was chosen because it was clear from studying experimental data that a bilinear model would not describe the stress-strain response very well.[3] By looking at cyclic data, it could also be seen from comparing the first, fifth, tenth, fortieth, and two-hundredth cycles that the material had a limited memory; that is, all these cycles looked very similar.

6.1 Development of the Material Model

The development is limited here to isothermal conditions. The yield condition is presently taken to be of the form

$$f(\sigma_{ij}, \alpha_{ij}) = \kappa , \tag{1}$$

where σ_{ij} are components of the stress tensor and α_{ij} are components of the translation tensor, specifying kinematic translations of the yield surface. For a fixed *inelastic state*, that is, fixed α_{ij} and κ, Eq. (1) is interpretable, in the usual way, as a hyper-surface in stress space that separates stress points for which plastic deformation takes place from those for which only elastic deformations occur.

The isotropic-hardening rate is specified by

$$d\kappa = g_{ij} \, (\sigma_{k\ell}, \varepsilon^p_{k\ell}) \, d\varepsilon^p_{ij} , \tag{2}$$

which, in general, depends on stress and plastic strain. Also, $d\kappa = 0$ when $d\varepsilon^p_{ij} = 0$.

The kinematic-hardening rate is likewise specified as

$$d\alpha_{ij} = G_{ijk\ell} (\sigma_{rs}, \varepsilon^p_{rs}) \, d\varepsilon^p_{k\ell} \ . \qquad (3)$$

Once again, $d\alpha_{ij} = 0$ when $d\varepsilon^p_{ij} = 0$.

The unique *isotropic* form of Eq. (3) with $d\varepsilon^p_{ij} = d\varepsilon^p_{ji}$ and $d\varepsilon^p_{kk} = 0$ is

$$d\alpha_{ij} = G \, (\sigma_{k\ell}, \varepsilon^p_{k\ell}) \, d\varepsilon^p_{ij} \ , \qquad (4)$$

in which G is a scalar function. This form will be adopted here, meaning that, in the present case, the center of the yield surface always translates in the direction of the plastic strain increment.*

From a given inelastic state with $f = \kappa$, an infinitesimal stress increment $d\sigma_{ij}$ such that $\frac{\partial f}{\partial \sigma_{ij}} d\sigma_{ij} > 0$ (loading) causes a plastic strain increment

$$d\varepsilon^p_{ij} = \lambda \frac{\partial f}{\partial \sigma_{ij}} \ . \qquad (5)$$

Equation (5) expresses the usual *normality* condition. As loading occurs (i.e., $d\varepsilon^p_{ij} \neq 0$, $d\kappa \neq 0$, and $d\alpha_{ij} \neq 0$), the stress point must remain on the yield surface; this is ensured through satisfaction of the consistency condition, that is,

$$df = d\kappa \ . \qquad (6)$$

Using Eqs. (1), (2), and (4), this condition gives

$$\frac{\partial f}{\partial \sigma_{ij}} d\sigma_{ij} + \frac{\partial f}{\partial \alpha_{ij}} G \, d\varepsilon^p_{ij} = g_{ij} \, d\varepsilon^p_{ij} \ . \qquad (7)$$

---

*Equation (4) provides a good idealization of the kinematic-hardening behavior for proportional and near proportional loading. It is assumed here (however, not tested) that Eq. (4) also provides a reasonable first-order approximation for general loading.

Now, using Eq. (5), we get the flow law

$$d\varepsilon_{ij}^{p} = \lambda \frac{\partial f}{\partial \sigma_{ij}} = \left[\frac{\dfrac{\partial f}{\partial \sigma_{k\ell}} \, d\sigma_{k\ell}}{\dfrac{\partial f}{\partial \sigma_{rs}} \left(g_{rs} - G \dfrac{\partial f}{\partial \alpha_{rs}} \right)} \right] \frac{\partial f}{\partial \sigma_{ij}} \; . \tag{8}$$

At this point, we shall adopt specific forms of the above equations. The yield conditions [Eq. (1)] will be taken as

$$f = \frac{1}{2} (s_{ij} - \alpha_{ij})(s_{ij} - \alpha_{ij}) = \kappa \; , \tag{9}$$

in which s_{ij} denotes the components of the stress deviator, that is, $s_{ij} = \sigma_{ij} - \frac{1}{3} (\sigma_{kk}\delta_{ij})$. Note that when $\alpha_{ij} = 0$, $f = J_2 \equiv \frac{1}{2} s_{ij}s_{ij}$, and Eq. (9) becomes the familiar von Mises yield condition. In Eq. (2), g_{ij} will be taken as

$$g_{ij} = Hs_{ij} \; , \tag{10}$$

in which H is a scalar function.

Equation (2) thus becomes

$$d\kappa = Hs_{ij}d\varepsilon_{ij}^{p} = H(W)dW \; , \tag{11}$$

in which W represents the inelastic work,

$$W = \int s_{ij} d\varepsilon_{ij}^{p} \; .$$

With these explicit forms, Eq. (8), the flow law, becomes

$$d\varepsilon_{ij}^{p} = \frac{(s_{k\ell} - \alpha_{k\ell})(s_{ij} - \alpha_{ij}) \, d\alpha_{k\ell}}{(s_{rs} - \alpha_{rs})[Hs_{rs} + G\,(s_{rs} - \alpha_{rs})]} \; . \tag{12}$$

Now, if we assume that the denominator of Eq. (12) is a function of κ only, that is,

$$(s_{ij} - \alpha_{ij})[Hs_{ij} + G\,(s_{ij} - \alpha_{ij})] = F(\kappa) \ , \tag{13}$$

or, in particular, if we take

$$F(\kappa) = (\beta/\kappa)^n \tag{14}$$

in which β and n are constants, we get for the kinematic-hardening function G:

$$G = \frac{(\beta/\kappa)^n}{2\kappa} - \frac{H}{2\kappa}\, s_{ij}\,(s_{ij} - \alpha_{ij}) \ . \tag{15}$$

The kinematic-hardening rate itself thus becomes

$$d\alpha_{ij} = \left[\frac{(\beta/\kappa)^n}{2\kappa} - \frac{H}{2\kappa}\, s_{k\ell}\,(s_{k\ell} - \alpha_{k\ell})\right] d\varepsilon^p_{ij} \ . \tag{16}$$

Making use of Eqs. (12)–(14), we can write Eq. (16) as:

$$d\alpha_{ij} = \frac{(\beta/\kappa)^n}{2\kappa}\, d\varepsilon^p_{ij} - \frac{d\kappa}{2\kappa}\,(s_{ij} - \alpha_{ij}) \ . \tag{17}$$

Note that with $n = -1$ and $\beta = \frac{1}{2C}$, Eq. (17) reduces to

$$d\alpha_{ij} = C\, d\varepsilon^p_{ij} - \frac{d\kappa}{2\kappa}\,(s_{ij} - \alpha_{ij}) \ . \tag{18}$$

This corresponds to the situation in which there are both isotropic and kinematic hardening, and the uniaxial stress-plastic strain curve is *linear* with slope $E_p = \frac{3C}{2}$.

If, in addition, $H = 0$, that is, there is no isotropic hardening, Eq. (18) further reduces to

$$d\alpha_{ij} = C\, d\varepsilon^p_{ij} \ , \tag{19}$$

the classical *linear kinematic*-hardening model of Prager.

6.2 Special Considerations for Stress Reversals

At an indication of *reversed plastic strain*, that is, when, in a stepwise calculation, the calculated increment in plastic strain $d\varepsilon^p_{ij}$ has a component in a direction opposite to the plastic strain increment last calculated, two measures are taken.

1. The yield parameter κ, whose growth rate is given by Eq. (11), is reset to κ_o, its value in the undeformed state.*

2. The current value of inelastic work, measuring the inelastic *state* of the material, is reduced by an amount of $\delta(\int dW, \Delta W)$, where δ is considered a function of the total accumulated inelastic work $\int dW$ and that amount accumulated since the last inelastic reversal ΔW.

These measures are in keeping with the viewpoint discussed in the introduction of the analytical method and procedures; that is to say, κ is reset, erasing its contribution to the recorded memory of deformation history, whereas the state variable W is partially reset by an amount that depends on the *total* accumulated inelastic work (i.e., an accumulative measure of the complete history of deformation).

6.3 The Model Adapted to 9 Cr-1 Mo Steel

In the derivation just discussed, the previously unspecified functions H and δ were taken as follows:

$$H(W) = \frac{A}{(1 + W/B)^2} , \qquad (20)$$

$$\delta(W^T, \Delta W) = \left[c + (1 - c)\left(1 - e^{W^{T/Z}}\right)\right] \Delta W , \qquad (21)$$

in which $W^T = \int dW$ and A, B, and Z are constants.

---

*For the stress point to remain on the yield surface, this abrupt change in κ must be accompanied by a corresponding jump in α_{ij}. Thus, according to Eq. (17), we have for consistency:

$$\Delta\alpha_{ij} = -\frac{\kappa - \kappa_o}{2\kappa}(s_{ij} - \alpha_{ij}) .$$

Using the definition given by Eq. (20), Eq. (11) is integrated and becomes

$$\kappa = \kappa_o + \int \frac{AdW}{(1 + W/B)^2} \ . \qquad (22)$$

As before, κ_o is the initial value of κ, and W is the value at the end of the integration interval.

Remembering that Ep = 3/2 C and using Eq. (17) and (18), the plastic modulus can be written as

$$E_p = \frac{3}{4} \frac{\beta}{\kappa^{n+1}} \ . \qquad (23)$$

To qualitatively represent the elastic-plastic behavior of modified 9 Cr-1 Mo steel (heat 30388) between 427 and 593°C (800 and 1100°F), the following material parameters were chosen:

$A = aF,$

$B = b/F,$

$Z = \Omega/F,$

$\kappa_o = K/F,$

$\beta = \gamma E \kappa_o^{n+1},$

where

$a = 8 \times 10^6,$

$b = 15.0,$

$c = 1.0,$

$n = 0.15,$

$\Omega = 750.0,$

$\kappa = 3 \times 10^6,$

$\gamma = 17.6,$

$F = 9.6612 \times 10^{-7} T^{1.9268},$

$E = 8.5933 \times 10^9 T^{-0.8586}.$

F is a function of temperature (°F), and E is the elastic modulus (psi) as a function of temperature (°F).

These parameters were based on an analysis of test data obtained on modified 9 Cr–1 Mo steel under a subcontract with Battelle–Columbus Laboratories. Cyclic stress–strain data were collected at three different temperatures: 427, 510, and 593°C (800, 950, and 1100°F). The data used for the development of the plasticity model were collected under continuous cycling for 200 cycles. Specifically, six continuous cycling experiments were done under fully reversed strain conditions at a total strain range of 0.40% and at a strain rate of 0.005 min^{-1}. Each experiment was started in the tensile strain direction, and the initial stress–strain curve was recorded. Two experiments were done at each temperature.

The nonlinear, time-independent plasticity model for the constitutive equations was programmed into the ADINA (Ref. 1) computer code. The computer code was used to analyze a simple uniaxial 2-1/4 cycle problem, which was then compared with a simple uniaxial analysis done through standard (non-finite-element) numerical integration of the nonlinear plasticity model. (The nonlinear plasticity model was compared with experimental data in Ref. 3. The comparison was for the tenth cycle and was very good.) The comparison between the ADINA and the standard solution for uniaxial cycling of the nonlinear model is shown in Fig. 8. This comparison, in general, fits the tip-to-tip stress and the cyclic shape of the curves.

6.4 Creep Relation

The creep equation describing uniaxial constant stress vs time data is taken from Ref. 4. The equation is a rational polynomial plus steady state form written as

$$\varepsilon^c(\sigma,t) = \frac{CPt}{1 + Pt} + \dot{\varepsilon}_m \ , \qquad (24)$$

where

$$\log \dot{\varepsilon}_m = 23.403 + 0.02292\sigma + 3.98 \log \sigma - \frac{33{,}610.0}{T} \ ,$$

$$C = 1.38 \ \dot{\varepsilon}_m^{\,0.15} \ , \qquad (25)$$

$$P = 4.61 \ \dot{\varepsilon}_m^{\,0.57} \ ,$$

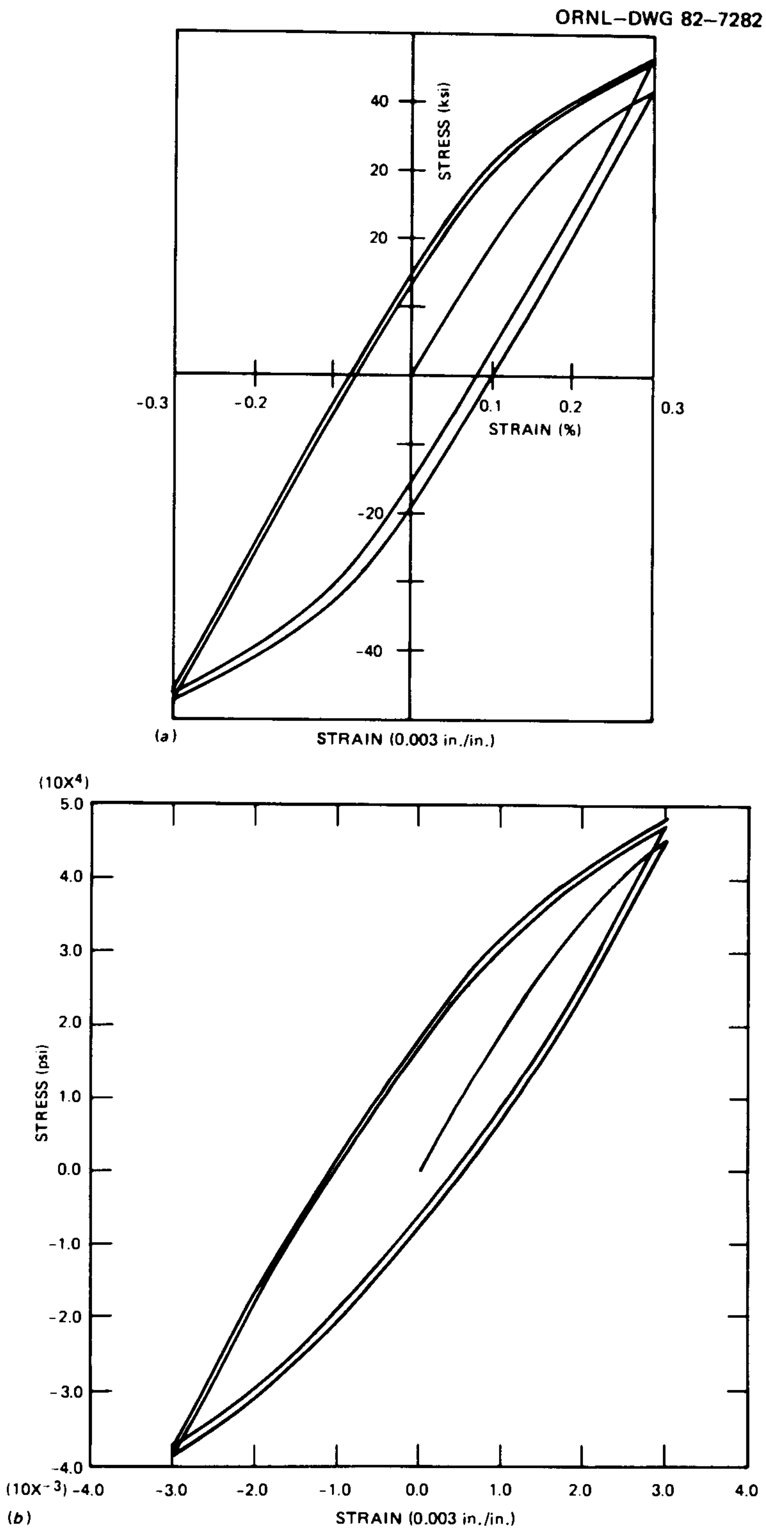

Fig. 8. Comparison between ADINA code and nonlinear plasticity model for a simple uniaxial cyclic problem.

with σ in megapascals as stress, t in hours as time, and $\dot{\varepsilon}_m$ in percent per hour. The creep strain ε^c is in percent.

This creep equation was used in the creep constitutive equations developed for the strain-hardening model given in Nuclear Standard NE F 9-5T (Ref. 5) for the finite-element analysis.

6.5 The Finite-Element Analysis

The analysis reported in the main body of this report was performed using the computer program ADINA (Ref. 1). The beam specimen and its finite-element idealization are shown in Fig. 9. A plane-stress eight-node isoparametric quadrilateral element was used in the analysis. Quarter symmetry was employed for the beam model. The deflection loading was applied at the center. Six elements were used in the quarter symmetrical

ORNL-DWG 82-5537ETD

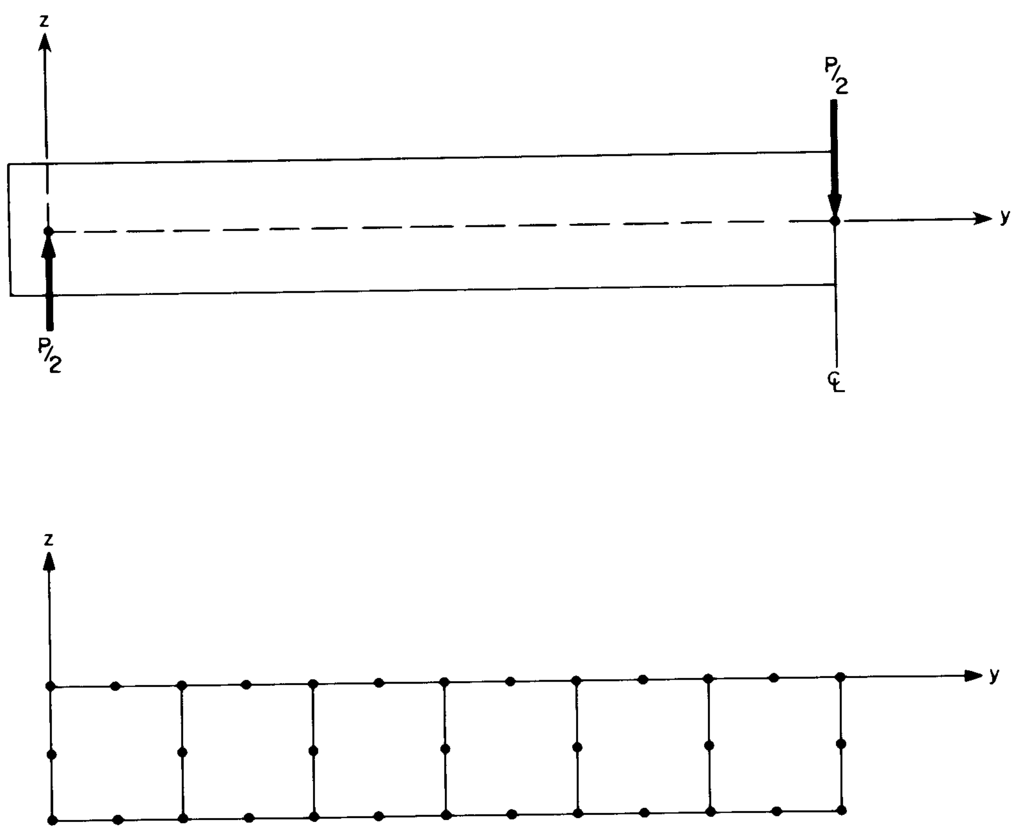

Fig. 9. Finite-element idealization of beam.

model with each element containing eight nodes and nine integration points. The finite-element solution used a Gaussian integration procedure to evaluate the stiffness, strain, stress, and displacements. The solution was calculated in the standard incremental elastic-plastic tangent-stiffness procedures used in the ADINA code.

The beam was loaded by a histogram of center deflection, and the resulting test response parameters were load (center load) and strains. To compare the calculated center load with the measured center load, a procedure had to be developed to calculate a load from the beam stresses. The moment in the beam at the center was calculated by integrating the following:

$$M = \int_{-h/2}^{h/2} \sigma \, ZdA = b \int_{-h/2}^{h/2} \sigma \, ZdZ \ , \tag{26}$$

where M = moment, σ = stress, b = width of beam, and h = thickness of beam. Then the load P was calculated by

$$P = \frac{4M}{L} \ , \tag{27}$$

where L is the length of the beam.

Equation (26) was numerically integrated by using an adoptive quadrature Newton-Cotes eight-panel integration described in Ref. 6. To use this numerical procedure, the row of integration points (three points) adjacent to the center of the beam in the finite element close to the beam center was used to integrate Eq. (26). To form the function used in Eq. (26), a cubic spline function[7] was fitted to the stress for a function of stress vs thickness Z. The spline function allowed the three integration points, even when the stress was very nonlinear with respect to thickness, to be accurately integrated in Eq. (26). For each time step, an integration of Eq. (26) was done, giving a calculated moment M and load P.

To compare the measured strain with the calculated strain, the strains at the nine integration points in the finite element close to the center were extrapolated to the position of the capacitance strain gage.

This was done by fitting a cubic spline function to the strain for a function of strain vs length (Y at constant Z), or thickness dimensions, which gave three spline functions for strain vs Y or length dimension. These three functions were used to evaluate the strain at the Y dimension of the strain gage for each of the three Z dimensions. The three new calculated values of strain were fitted by a cubic spline function to form a function of strain vs Z or thickness dimension. The new strain vs Z function was used to calculate the strain at the surface at the strain-gage position. The calculation was done for each time step, giving a calculated strain at surface for each time step.

7. COMPARISONS OF ANALYTICAL AND EXPERIMENTAL RESULTS

The comparisons between predictions and experiment are shown graphically in this section. The numbered points on the histogram in Fig. 7 and the nomenclature given in Fig. 2 are used to describe the load steps. The first comparison will be the first loading of the beam shown between the points 0 and 1 on the histogram. Figure 10 compares the load vs center deflection for this first loading of the beam. The comparison is good. Figure 11 shows the comparison between the strains vs load as measured by the two strain gages on the beam. The gages compare favorably with each other and with the analytically calculated strain. Figure 12 shows the comparisons of DCDTs, which are 10.16 cm (4 in.) from the center (symmetrical about the center with the analytical results). The comparisons are very good, which indicates that at the beginning of the test, the loading was symmetrical and the beam performed in a symmetrical fashion.

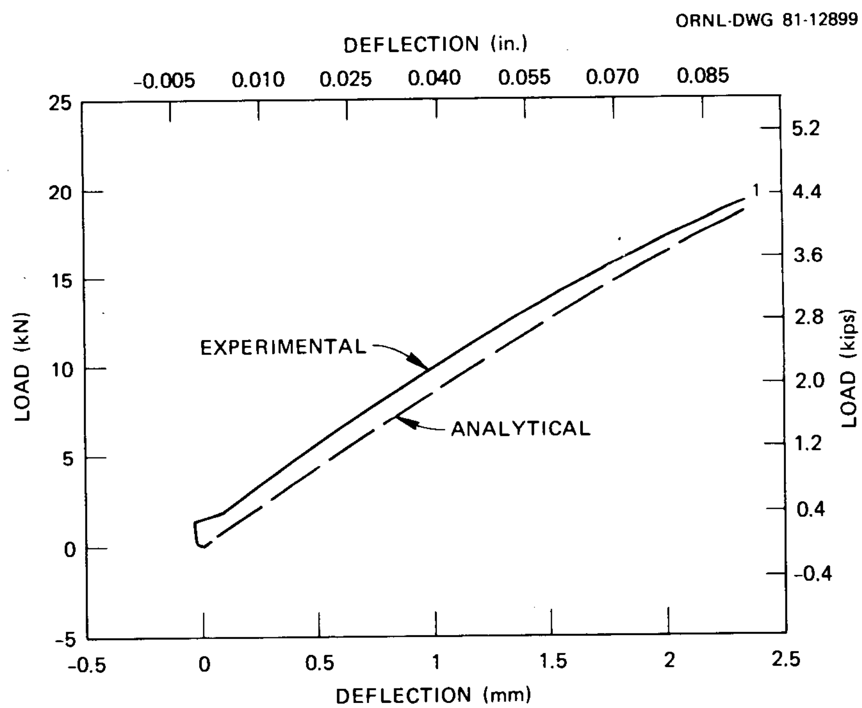

Fig. 10. Measured and predicted center deflection vs center load of DCDT-4. Numbered points refer to histogram in Fig. 7.

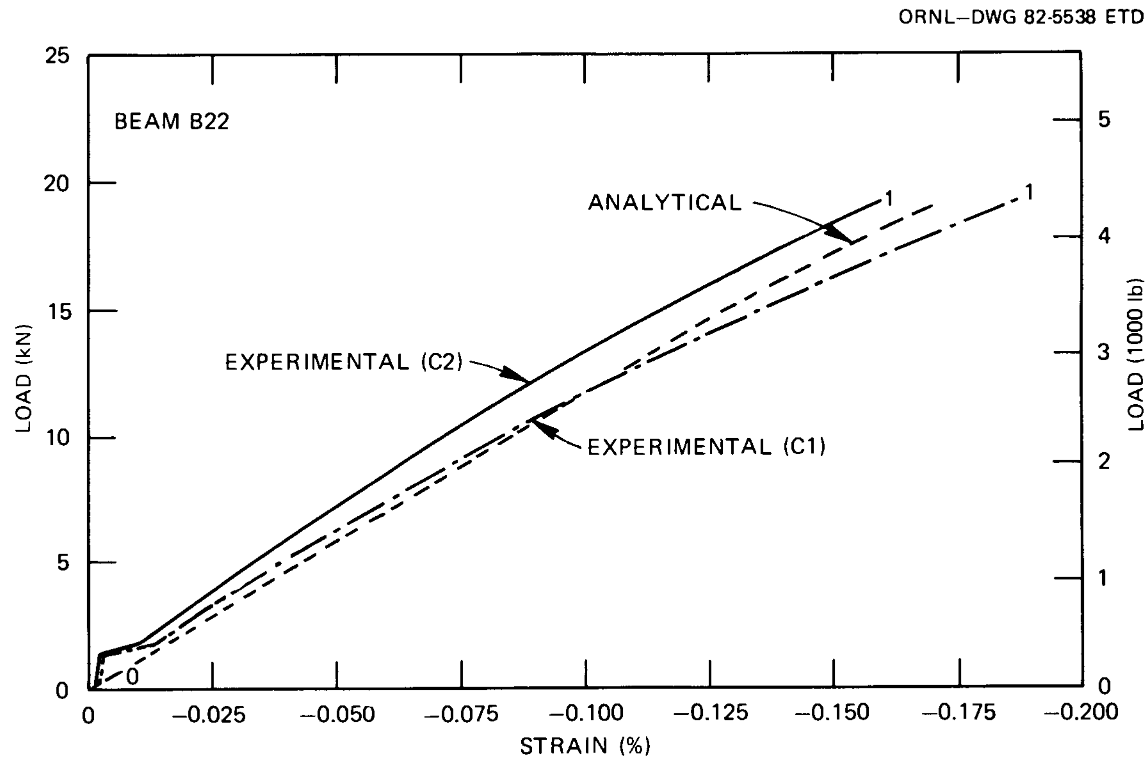

Fig. 11. Measured and predicted strain vs center load of strain gages C1 and C2. Numbered points refer to histogram in Fig. 7.

Plots of total load vs time are presented in Fig. 13 for the center displacement transducer (DCDT-4). Figure 13(*a*) shows the experimental results, and Fig. 13(*b*) shows the analytical results. The figures indicate that the total load over the entire 504-h test was reasonably well predicted, and quantitative agreement is generally good.

Plots of total load vs center deflection are shown in Fig. 14, and plots of the time-dependent center load vs time are shown in Fig. 15. These plots show that the time-dependent (creep) deflections are reasonably well predicted. Plots of time-independent center load vs deflection are shown in Figs. 16 and 17, with Fig. 17 being an overlay comparison. From these figures, the inelastic (nonlinear) responses to loadings agree in magnitude for the cyclic loadings and in shape, particularly in the loading and unloading portions of the cyclic loops.

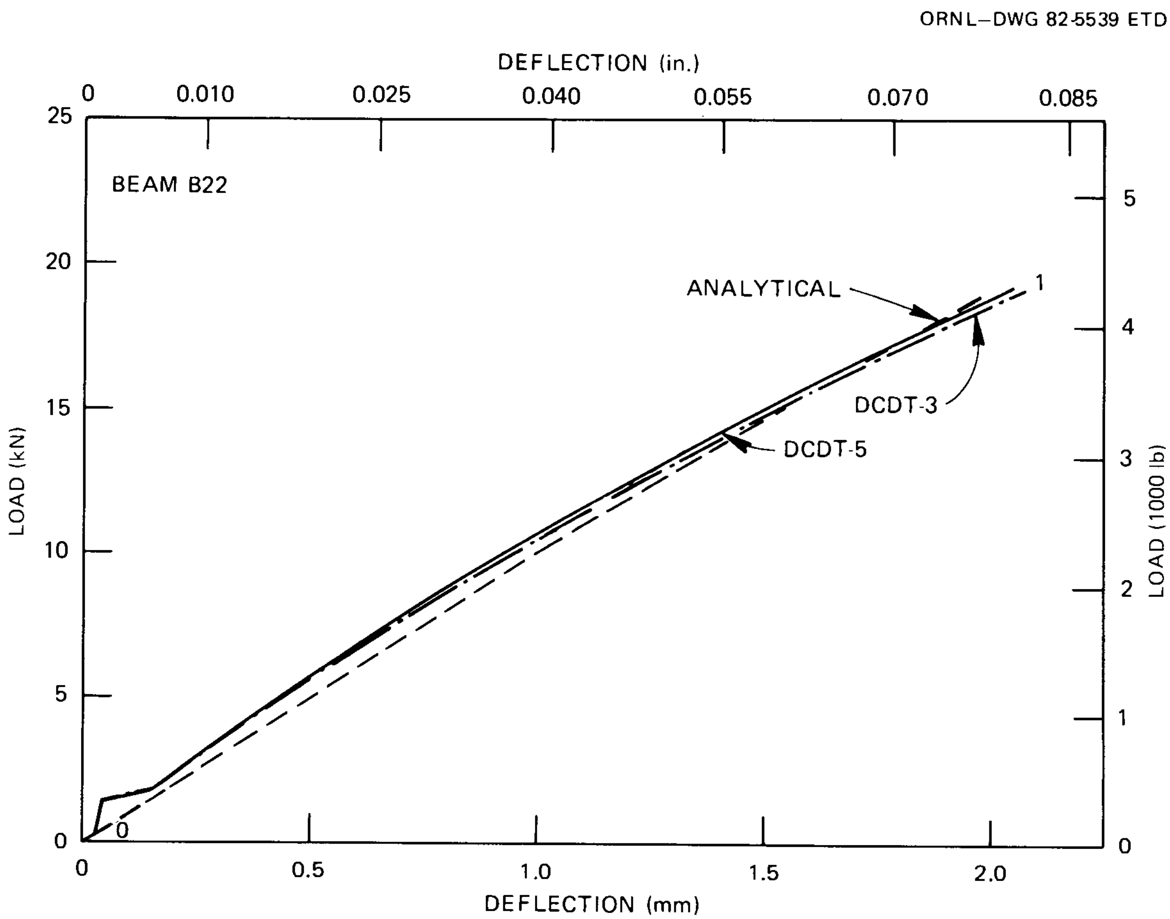

Fig. 12. Measured and predicted deflection vs center load of DCDT-3 and -5. DCDTs are 10 cm (4 in.) from the center. Numbered points refer to histogram in Fig. 7.

ORNL–DWG 82–5540 ETD

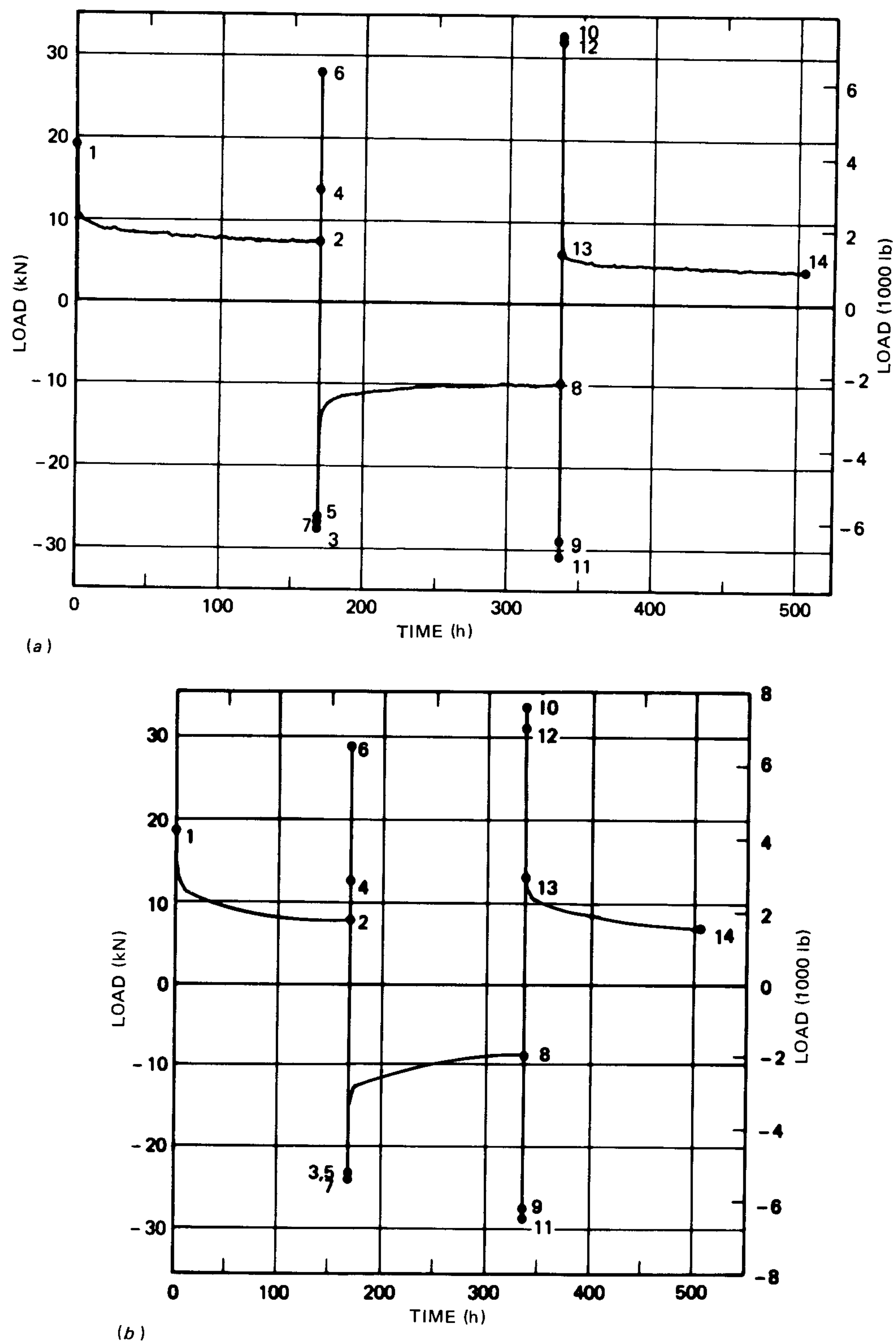

Fig. 13. Comparison of measured and calculated total center load vs time. Numbered points refer to histogram in Fig. 7.

ORNL–DWG 82–5541 ETD

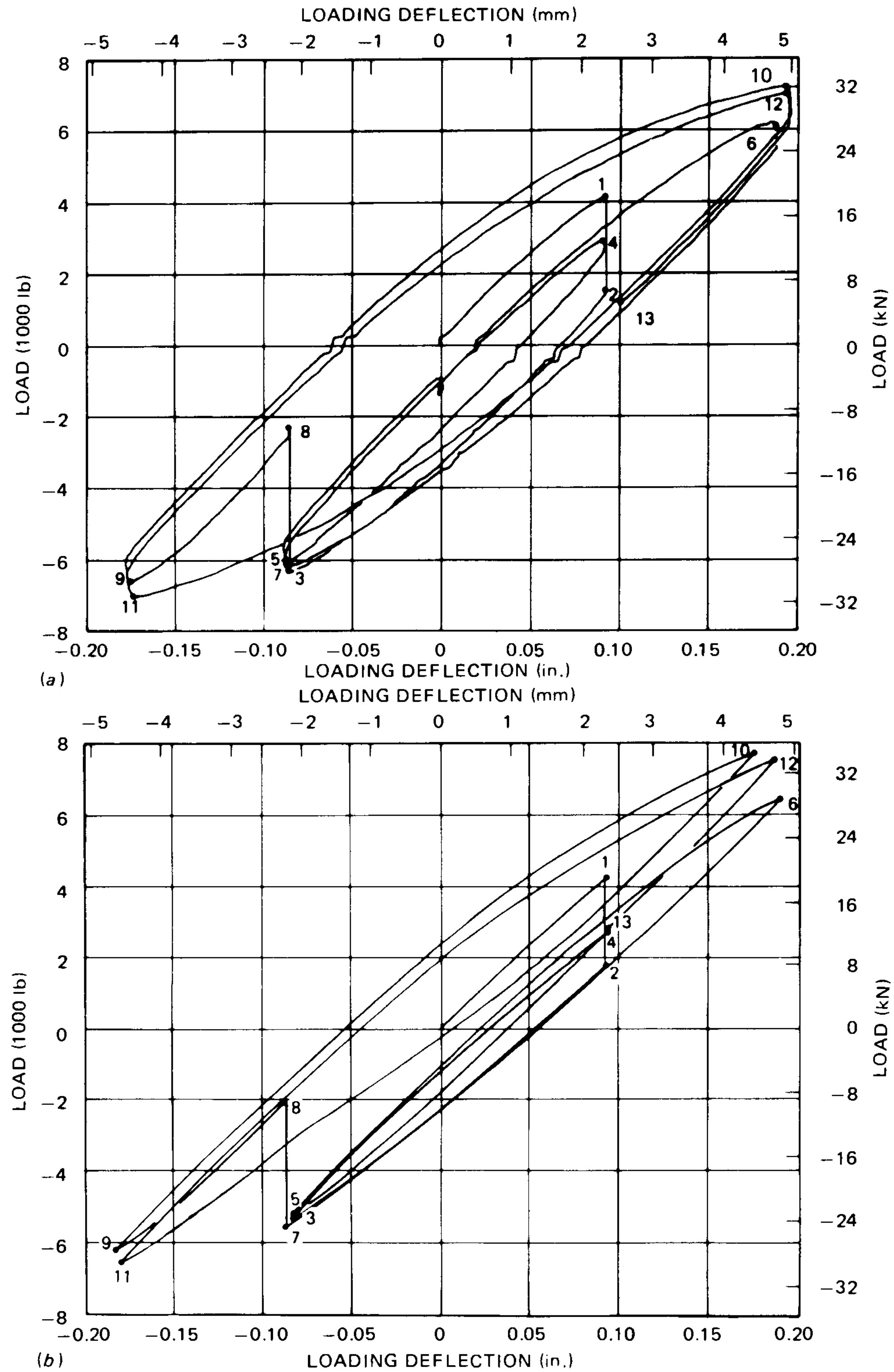

Fig. 14. Comparison of measured and calculated total center load vs deflection. Numbered points are defined in histogram in Fig. 7.

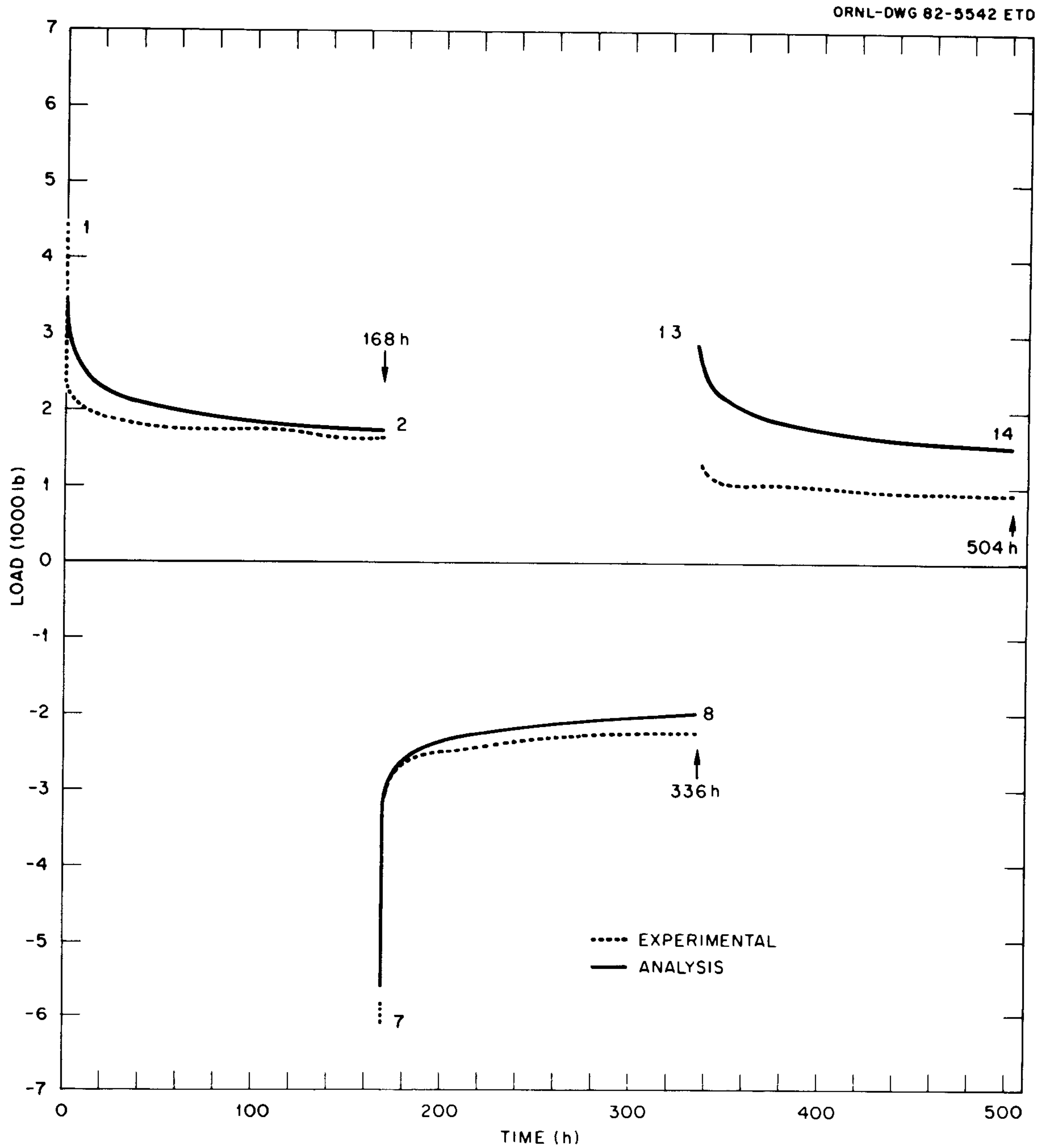

Fig. 15. Comparisons of measured and calculated center time-dependent load vs time. Numbered points are defined in histogram in Fig. 7.

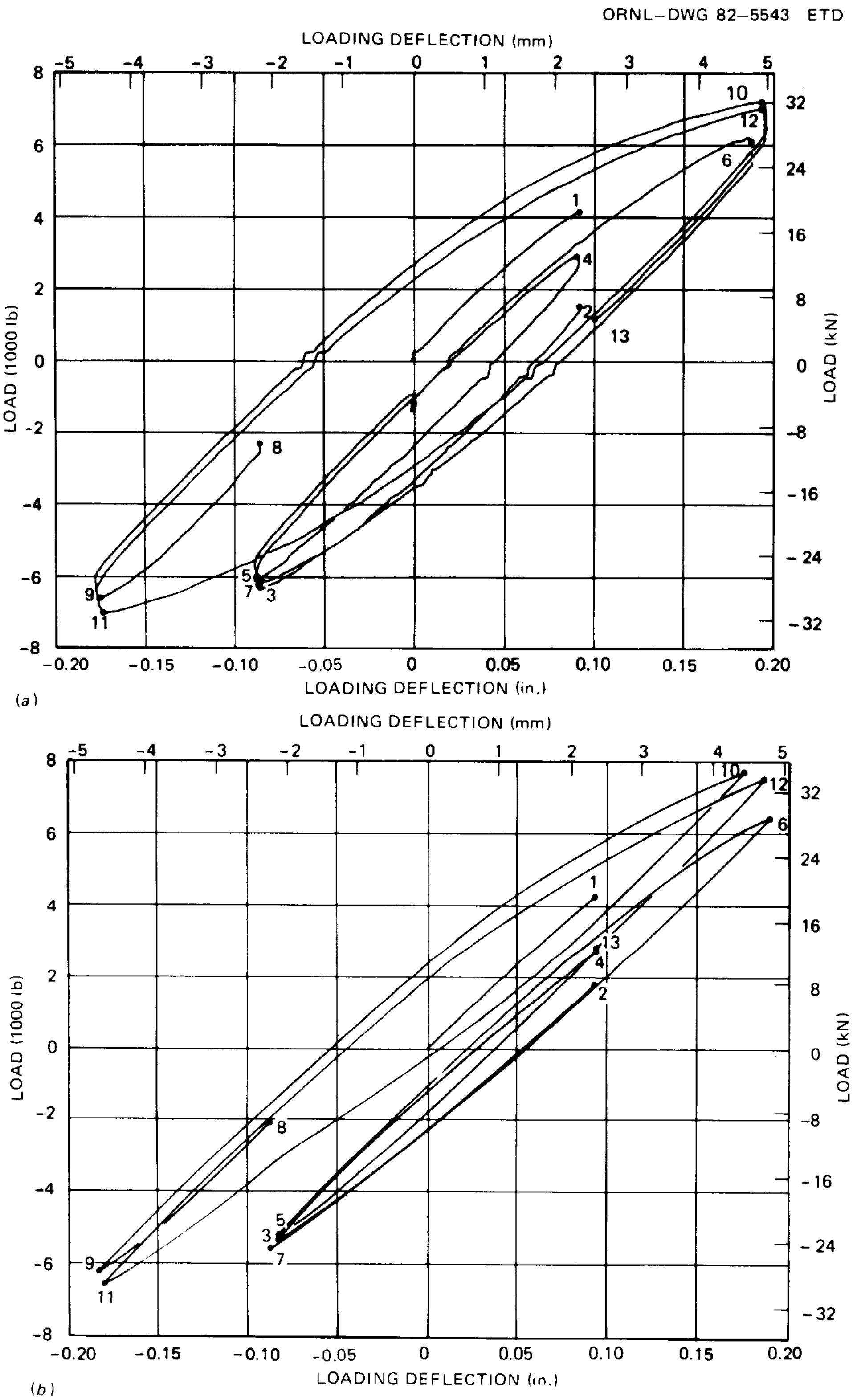

Fig. 16. Comparison of measured and calculated center time-independent load vs deflection. Numbered points are defined in histogram in Fig. 7.

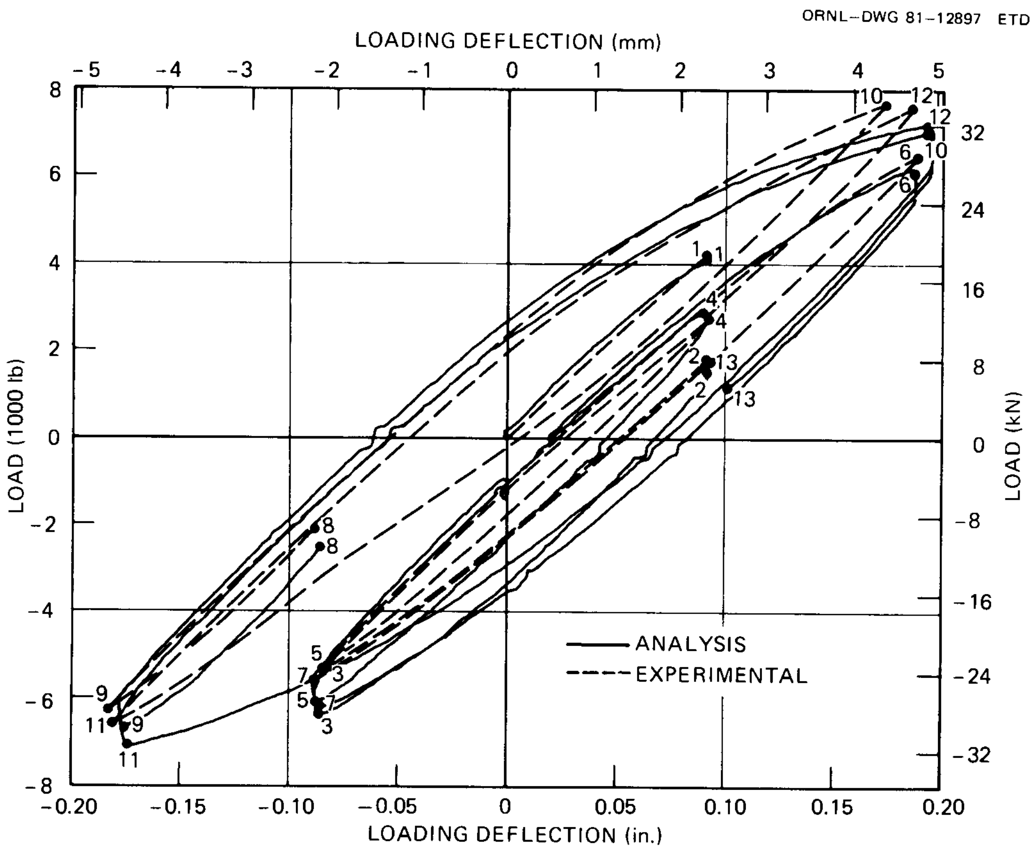

Fig. 17. Overlay comparison of measured and calculated center time-independent load vs deflection. Numbered points are defined in histogram in Fig. 7.

8. DISCUSSION AND SUMMARY

The analytical method was able to predict the magnitude of the loading and the general shape of cyclic curves during the test. The creep relaxation was predicted very well in its magnitude and time-dependent shape. The only shortcoming between the analytical and experimental results was the apparent creep relaxation that occurred at the end of the experimental cyclic loops. If this creep relaxation does actually occur at the end of the loops, its prediction might require that a "unified" constitutive equation theory be used or that the analysis be modified to allow creep to occur during load changes. These possibilities will be further examined.

9. ACKNOWLEDGMENTS

The authors gratefully acknowledge the help of S. J. Claiborne in instrumenting the specimen and performing the test. Also D. T. Godwin's help in preparation of the figures for the report is gratefully acknowledged. D. N. Robinson provided the nonlinear plasticity theory used, and J. A. Clinard performed the confirmatory analysis given in the appendix.

REFERENCES

1. Klaus-Jurgen Bathe, *ADINA — A Finite Element for Automatic Dynamic Incremental Nonlinear Analysis*, Massachusetts Institute of Technology, Report 82448-1 (September 1975).

2. D. N. Robinson, *A Nonlinear Plasticity Model for Structural Alloys at Elevated Temperature*, ORNL/TM-6582 (November 1978).

3. R. C. Gwaltney and G. T. Yahr, *A Preliminary Analytical Assessment of the Structural Performance of Modified 9 Cr—1 Mo Steel Relative to Other Alloys in FBR Applications*, presented at USDOE/CEA/DEBENE Exchange Meeting on Alternate Steam Generator Structural Materials for Fast Breeder Reactor Service, Oak Ridge National Laboratory, Oak Ridge, Tenn., ORNL/TM-7586 (October 1980).

4. V. K. Sikka, Oak Ridge National Laboratory, personal communication to J. M. Corum, Oak Ridge National Laboratory, March 27, 1980.

5. *Guidelines and Procedures for Design of Class 1 Elevated Temperature Nuclear System Components*, NE F 9-5T, pp. 97—96, March 1981.

6. G. E. Forsythe, M. A. Malcolm, and C. B. Moler, *Computer Methods for Mathematical Computations*, pp. 97—105, Prentice-Hall, 1977.

Appendix

A CONFIRMATORY ANALYSIS

A second analysis of the modified 9 Cr–1 Mo beam was done using the ORNL in-house computer program CREEP-PLAST II.* This program uses the three-node, linear-displacement, constant-strain triangle and axisymmetrical revolved-triangle elements. A plane-stress three-node constant-strain triangle was used in the analysis. Quarter symmetry was employed for the beam model. The deflection was applied at the center. The finite-element model contained 256 elements and 165 nodes (see Fig. A.1). The solution was calculated with the standard incremental elastic-plastic tangent-stiffness procedure used in the CREEP-PLAST II code, and the constitutive equations described in the body of the report were used.

In this analysis, the beam was loaded by a histogram of nominal deflection (deflections that were planned for the test but were not necessarily actually reached or obtained). Therefore, this analysis is not an exact analysis of the test. The CREEP-PLAST II code calculates the load directly, and the calculated load vs deflection is shown in Fig. A.2 for load points 0–11. As can be seen, the results are very similar to the calculated results shown in Fig. 14(*b*) (Sect. 7). This analytical method was able to predict the general shape and sense of the cyclic curves even though the magnitudes were not exactly calculated because of using the nominal deflections. This independent analysis thus helps to verify the ADINA analysis. It seems that at the end of each experimental loop [Figs. 14(*a*), 16(*a*), and 17], there is stress relaxation. At present it is not known whether this relaxation actually does occur or if it is some kind of experimental problem or movement in the mechanical instrumentation during the experiment.

---

*J. A. Clinard, *CREEP-PLAST II User's Manual*, ORNL/TM-5868 (May 1978).

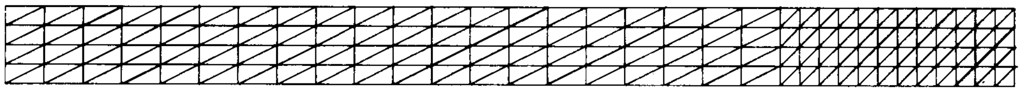

Fig. A.1. CREEP-PLAST II finite-element idealization of beam. One-quarter symmetry was used.

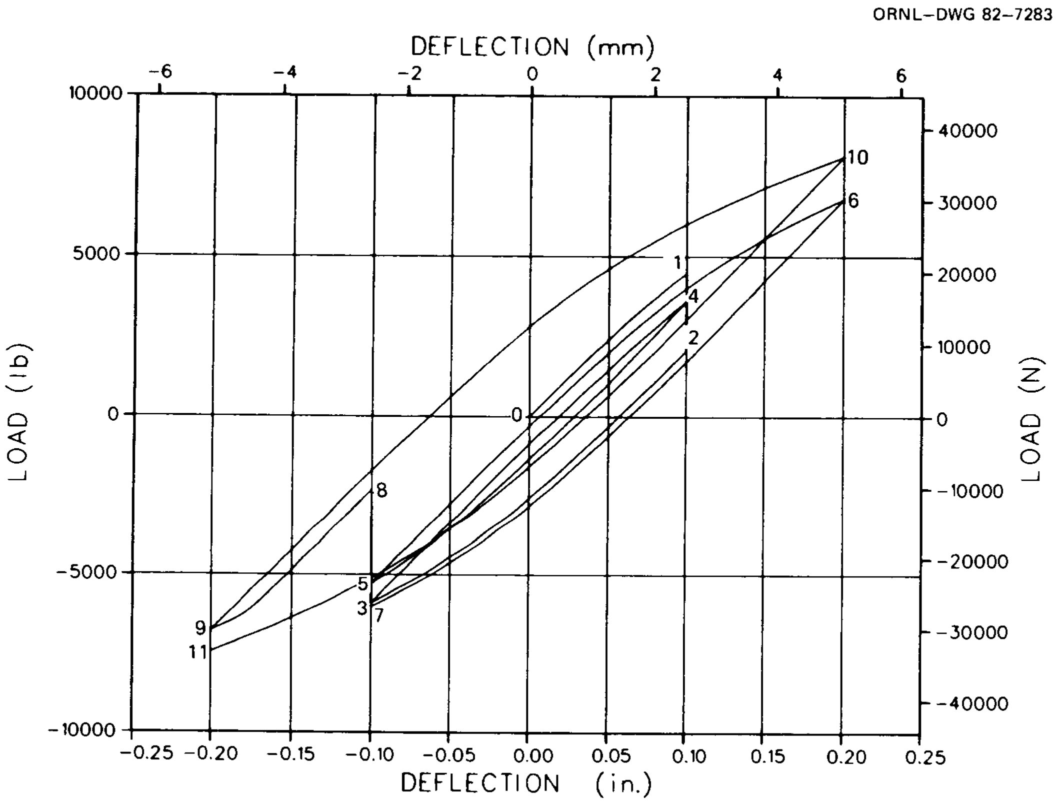

Fig. A.2. Calculated total center load vs center deflection by CREEP-PLAST II code. Numbered points are defined in histogram in Fig. 7.

ORNL/TM-8254
Dist. Category UC-79T,
-79Th, -79Tk

Internal Distribution

1. R. L. Battiste
2. J. J. Blass
3. C. R. Brinkman
4. J. A. Clinard
5-9. J. M. Corum
10. L. B. Dockery
11. J. R. Ellis
12. D. T. Godwin
13. W. L. Greenstreet
14. D. S. Griffith
15-19. R. C. Gwaltney
20. R. L. Huddleston
21. Y. L. Lin
22. W. J. McAfee
23. S. E. Moore
24. C. E. Pugh
25. W. K. Sartory
26. R. W. Swindeman
27. H. E. Trammell
28. M. D. Weaver
29-31. G. T. Yahr
32. ORNL Patent Office
33. Central Research Library
34. Document Reference Section
35-36. Laboratory Records Department
37. Laboratory Records, RC

External Distribution

38-39. Director, Office of Breeder Technology Projects, Department of Energy, Washington, DC 20545
40. Office of Assistant Manager for Energy Research and Development, Department of Energy, ORO, Oak Ridge, TN 37830
41-174. Given distribution as shown in DOE/TIC-4500 under categories UC-79T (Liquid-Metal Fast Breeder Reactors, UC-79Th (LMFBR — Structural Materials and Design Engineering), UC-79Tk (LMFBR — Components)